

2002064501
573060
26/5To appear in *The Astrophysical Journal*, Dec. 20, 2001

The Ionization and Metallicity of the Intervening O VI Absorber at $z = 0.1212$ in the Spectrum of H1821+643¹

Todd M. Tripp,² Mark L. Giroux,^{3,4} John T. Stocke,³ Jason Tumlinson,³ and William R. Oegerle^{5,6}

ABSTRACT

We use high-resolution UV spectra of the radio-quiet QSO H1821+643 ($z_{\text{em}} = 0.297$), obtained with the Space Telescope Imaging Spectrograph (STIS) and the *Far Ultraviolet Spectroscopic Explorer* (FUSE), to study the ionization and metallicity of an intervening O VI absorption line system at $z_{\text{abs}} = 0.1212$. This absorber has the following notable properties: (1) Several galaxies are close to the sight line at the absorber redshift, including an actively star-forming galaxy at a projected distance of $144 h_{75}^{-1}$ kpc. (2) There is a complex cluster of H I Ly α absorption lines near the O VI redshift, including at least five components spread over a velocity range of $\sim 700 \text{ km s}^{-1}$. (3) The strongest Ly α line in the cluster appears to be composed of a mildly saturated component with a typical b -value blended with a remarkably broad component with $b \approx 85 \text{ km s}^{-1}$. (4) The O VI absorption is not aligned with the strongest (saturated) H I absorption, but instead is well-aligned with the very broad component. (5) The only detected species (at the 4σ level) are O VI and H I despite coverage of strong transitions of abundant elements (e.g., C II, C III, and C IV). Based on these constraints, we find that the absorption line properties can be produced in collisionally ionized gas with $10^{5.3} \leq T \leq 10^{5.6} \text{ K}$ and $-1.8 \leq [\text{O}/\text{H}] \leq -0.6$. However, we find that photoionization is also viable if the pathlength l through the absorbing gas is long enough; simple photoionization models require $85 \leq l \leq 1900 \text{ kpc}$ and $-1.1 \leq [\text{O}/\text{H}] \leq -0.3$. We briefly discuss how observations of X-ray absorption lines due to O VII and O VIII could be used, in principle, to break the ionization mechanism degeneracy, and we conclude with some comments regarding the nature of O VI absorbers.

Subject headings: intergalactic medium — quasars: absorption lines — quasars: individual (H1821+643)

¹ Based on observations with the NASA/ESA *Hubble Space Telescope*, obtained at the Space Telescope Science Institute, which is operated by the Association of Universities for Research in Astronomy, Inc., under NASA contract NAS 5-26555.

² Princeton University Observatory, Peyton Hall, Princeton, NJ 08544, Electronic mail: tripp@astro.princeton.edu

³ Center for Astrophysics and Space Astronomy and Department of Astrophysical and Planetary Sciences, University of Colorado, Boulder, CO 80309.

⁴ Current address: Department of Physics and Astronomy, East Tennessee State University, Johnson City, TN 37614

⁵ Department of Physics and Astronomy, Johns Hopkins University, Baltimore, MD 21218

⁶ NASA Goddard Space Flight Center, Greenbelt, MD 20771

1. Introduction

Any successful cosmological model must account for the quantity, distribution, and physical state of the baryons in the Universe. While this is likely a more tractable challenge than understanding the more exotic non-baryonic dark matter and dark energy (i.e., the cosmological constant), there is a “missing baryon problem” which has been known for some time. In brief, inventories of the well-observed baryons in the nearby Universe (including stars, cool neutral gas, and X-ray emitting galaxy cluster gas) find total baryon densities, in units of the closure density, of $\Omega_b = \rho/\rho_c \approx 0.006$ (assuming $H_0 = 75h_{75} \text{ km s}^{-1} \text{ Mpc}^{-1}$, see, e.g., Persic & Salucci 1992; Fukugita et al. 1998). This is far less than the expected value based on Big Bang nucleosynthesis and deuterium measurements (Burles & Tytler 1998): $\Omega_b h_{100}^2 = 0.019 \pm 0.001$ ($= 0.034 \pm 0.002$ for $h_{100} = 0.75$). Ironically, the baryons have been more readily accounted for in the distant Universe than in the low- z Universe: at high redshifts, the “Ly α forest” – photoionized, diffuse intergalactic gas at $T \sim 10^4 \text{ K}$ – appears to contain the vast majority of the baryons predicted by the deuterium observations (Rauch et al. 1997; Weinberg et al. 1997). At low redshifts, the cool Ly α forest is less dominant but still makes a substantial contribution to the baryon inventory. However, even including recent estimates of the baryonic content of the low- z Ly α forest (Shull, Stocke, & Penton 1996; Penton, Shull, & Stocke 2000), the census of baryons at the present epoch falls well short of the expected Ω_b . Consequently, cosmologists are confronted with an important question: where are the missing baryons at the present epoch?

A promising possible answer to this question has been provided by cosmological simulations of the growth of large scale structure. According to hydrodynamic simulations of structure formation, at the present epoch 30–50% of the baryons (by mass) are located in low-density, intergalactic gas which has been shock-heated to $10^5 - 10^7 \text{ K}$ (Cen & Ostriker 1999a; Davé et al. 1999, 2001). Following Cen & Ostriker, we refer to this $10^5 - 10^7 \text{ K}$ gas as the warm/hot intergalactic medium to distinguish it from the hotter gas observed in rich galaxy clusters. Such gas is challenging to observe. Its X-ray emission is extremely difficult to detect, especially at lower energies where confusion due to foreground emission and absorption is substantial. Current X-ray observations do not exclude this hot IGM baryon reservoir (Kuntz, Snowden, & Mushotzky 2001; Phillips, Ostriker, & Cen 2001), and there are some indications of large-scale filaments of diffuse gas delineated by X-ray emission (e.g., Scharf et al. 2000; Rines et al. 2001). However, Voit, Evrard, & Bryan (2001) and Croft et al. (2001) have demonstrated that it is difficult to distinguish between X-ray emission from diffuse intergalactic gas outside of virialized structures (as predicted by the cosmological simulations) and X-ray emission from virialized groups and clusters. The gas may be a significant baryon repository in either case, but the distinction has important physical implications, e.g., regarding the relative importance of gravitational vs. nongravitational heating processes.

QSO absorption lines provide an alternative means to test the prediction that a significant quantity of baryons are in the warm/hot IGM. Absorption lines such as the O VI $\lambda\lambda 1031.9, 1037.6$ and Ne VIII $\lambda\lambda 770.4, 780.3$ doublets provide sensitive probes of $10^5 - 10^6 \text{ K}$ gas in collisional ionization equilibrium (Verner, Tytler, & Barthel 1994). Searches for the O VI absorption lines at $z_{\text{abs}} \lesssim 0.3$ with the Space Telescope Imaging Spectrograph (STIS) on board the *Hubble Space Telescope* (HST) have revealed that the number of intervening O VI absorbers per unit redshift (dN/dz) is remarkably high (Tripp, Savage, & Jenkins 2000; Tripp & Savage 2000). Furthermore, with reasonable assumptions about the metallicity and ionization of the gas, these studies have shown that O VI absorption systems are probably an important baryon reservoir.

Since the O VI ion fraction peaks at $T \sim 3 \times 10^5 \text{ K}$ in collisional ionization equilibrium, these O VI absorption studies provide tantalizing evidence that the warm/hot IGM is an important baryon repository

at $z \sim 0$. However, there are several issues which must be addressed in order to build a compelling case. First, the number of O VI systems (and sight lines) in the published STIS observations is rather small, and consequently quantities such as dN/dz and the cosmological mass density have large uncertainties. More observations are needed, and new programs to build the sample are underway. Second, the O VI lines could arise in gas which is not collisionally ionized, but rather is photoionized by the UV background from QSOs and active galaxies. Or, the gas could be collisionally ionized but out of equilibrium, e.g., because it is able to cool more rapidly than it can recombine. Photo- or non-equilibrium ionization is favored in some of the O VI systems because they have narrow associated H I lines (e.g., Tripp & Savage 2000; Savage et al. 2001) which would not arise in equilibrium collisional ionization. Alternatively, these could be multiphase absorbers. Of course, in some cases photoionization and collisional ionization could be comparably important. If the gas is photoionized, then there are concerns about double-counting in the baryon inventory (see below). Third, the metallicity of the absorbers is poorly constrained. If these O VI systems originate in pockets of high metallicity gas, then there is less hydrogen associated with the absorbers and their baryonic content is lower [$\Omega_b(\text{O VI}) \propto (\text{O}/\text{H})^{-1}$]. Finally, the environment in which these absorbers are located must be scrutinized. Are these absorbers found in unvirialized galaxy filaments or even galaxy voids, or do they arise in virialized structures? Are these systems due to gas which is gravitationally shock-heated when gas accretes onto large-scale structures, or could they be heated by nongravitational processes such as supernova-driven winds?

In this paper we are primarily interested in the ionization and metallicity of the gas. Specifically, we use high-resolution UV spectra obtained with STIS and the *Far Ultraviolet Spectroscopic Explorer (FUSE)* to study the ionization and nature of a particular absorption system at $z_{\text{abs}} = 0.1212$ in the spectrum of the radio-quiet QSO H1821+643 ($z_{\text{em}} = 0.297$). While some O VI absorbers are apparently “intrinsic” (i.e., close to the QSO itself, see Hamann & Ferland 1999), the H1821+643 absorber at $z_{\text{abs}} = 0.1212$ is certainly an intervening system: it is highly displaced from the QSO redshift ($\Delta v \approx 43,400 \text{ km s}^{-1}$) and is located at a redshift where there are several galaxies close to the line of sight, including a luminous galaxy at a projected distance of $144 h_{75}^{-1} \text{ kpc}$ which shows [O II], [O III], and $\text{H}\beta$ emission lines indicative of active star formation (Tripp, Lu, & Savage 1998; Bowen, Pettini, & Boyle 1998). The ionization mechanism is a crucial issue because if the O VI absorbers are photoionized and cool rather than collisionally ionized and hot, then they still represent a substantial baryon reservoir (see Tripp & Savage 2000), but in this case they may reveal the same baryons counted in $\text{Ly}\alpha$ studies such as Penton et al. (2000) [note that all intervening O VI systems that we have detected so far are also detected in the H I $\text{Ly}\alpha$ transition]. Apart from the baryon census, the metallicity and physical conditions of the gas are interesting in their own right.

The paper is organized as follows. The STIS and *FUSE* observations and data reduction are described in §2. Section 3 summarizes the absorption line measurement techniques. Constraints are placed on the physical conditions and metallicity of the gas in §4 including a comparison of the absorber properties required in collisionally ionized and photoionized scenarios and some comments on X-ray absorption lines of O VII and O VIII. We discuss the results and summarize our conclusions in §5. Throughout this paper we assume $H_0 = 75 \text{ km s}^{-1} \text{ Mpc}^{-1}$ and $q_0 = 0.0$ unless otherwise indicated. We also report heliocentric wavelengths and redshifts; in this direction, $v_{\text{LSR}} = v_{\text{helio}} + 16 \text{ km s}^{-1}$ assuming the standard definition of the local standard of rest (Kerr & Lynden-Bell 1986).

2. Observations and Data Reduction

This paper makes use of observations of H1821+643 taken with STIS in both the echelle and first-order grating modes, as well as shorter-wavelength observations made with the *FUSE* satellite. In this section we briefly describe the observations and data reduction; see Woodgate et al. (1998) and Kimble et al. (1998) for information on the design and performance of STIS, and Moos et al. (2000) and Sahnou et al. (2000) regarding the *FUSE* design and performance.

2.1. STIS Spectroscopy

H1821+643 was observed with the medium resolution FUV echelle mode (E140M) of STIS on 1999 June 25 and 2000 March 31 for a total integration time of 50.93 ksec. This STIS mode uses the FUV MAMA detector, which generally has very low dark background counts. While this detector also has an amoebic region that shows elevated dark counts when the detector temperature increases (see Figure 1 in Brown et al. 2000), the dark count rate was small compared to the source count rate for all of the observations employed here. The observations made use of the $0''.2 \times 0''.06$ slit resulting in a line spread function with minimal wings (see Figure 13.87 in the STIS Instrument Handbook, v4.1). This STIS echelle mode/slit combination provides a resolution of $R = \lambda/\Delta\lambda \approx 46,000$ (FWHM $\approx 7 \text{ km s}^{-1}$, see Kimble et al. 1998) and wavelength coverage from ~ 1150 to 1710 \AA with four small gaps between orders at $\lambda > 1630 \text{ \AA}$. Several STIS first-order grating observations of H1821+643 were also obtained on 1999 June 24. Most relevant to this paper is the STIS G230M observation extending from 1724 to 1814 \AA , which covers the C IV doublet at $z_{\text{abs}} = 0.1212$. This first-order grating spectrum has a resolution of $\sim 30 \text{ km s}^{-1}$ (FWHM).

The data were reduced with the STIS Team version of CALSTIS at the Goddard Space Flight Center. The individual echelle spectra were flatfielded, extracted, and wavelength and flux calibrated with the standard techniques. Then a correction for scattered light⁷ was applied using the method developed by Bowers et al. (2001), and the individual spectra were combined weighted by their inverse variances averaged over a large, high S/N region. Finally, overlapping regions of adjacent orders were also coadded weighted inversely by their variances.⁸ The first and last ten pixels in each order were not coadded to avoid spurious pixel values often seen near order edges.

The STIS G230M first-order grating observation covering the C IV $\lambda\lambda 1548.2, 1550.8$ doublet at $z_{\text{abs}} = 0.1212$ was flatfielded and wavelength calibrated in the normal way, but the spectrum was extracted with the optimal method of Robertson (1986). Two 50-pixel wide regions centered 52 pixels away from the spectrum (one on each side) were used to determine the background. The two G230M spectra were also combined with weighting based on signal- to-noise. To ensure that the wavelength scale of the G230M spectrum is aligned with that of the E140M echelle spectrum, the Milky Way Ni II $\lambda 1741.5$ and $\lambda 1751.9$ lines covered in the G230M spectrum were compared to the Milky Way Ni II $\lambda 1317.2$ and $\lambda 1370.1$ lines

⁷Inspection of the cores of strongly saturated lines indicates that while the scattered light correction is usually quite effective, occasionally errors in the flux zero point at the level of a few percent of the continuum are evident. Consequently, we have included a term due to the flux zero point uncertainty in the overall uncertainties in the STIS measurements (see §3), and we have allowed the profile-fitting code to adjust the zero point by a few percent (for the STIS data only) as a free parameter.

⁸For the overlapping regions of adjacent orders, the weighting was determined on a pixel-by-pixel basis. However, a five-pixel boxcar smoothing was applied to the error vectors for the determination of the weights so that pixels with larger noise fluctuations are not inappropriately over- or under-weighted.

recorded in the E140M spectrum.

2.2. FUSE Spectroscopy

H1821+643 was initially observed with *FUSE* on 1999 October 10 and 13; the total integration time was 48.8 ksec. Results from this observation have been presented by Oegerle et al. (2000). Subsequently, the QSO was re-observed with *FUSE* on 2000 July 24 with a total integration time of 62.7 ksec. Both observations used the large ($30'' \times 30''$) LWRS aperture. *FUSE* has four co-aligned telescopes and Rowland spectrographs which record spectra on two microchannel plate detectors. Two of the optical channels have LiF coatings to cover the 1000–1187 Å range, and the other two channels have SiC coatings to cover 905–1105 Å. During the 1999 October observation, only the two LiF channels were successfully aligned, but high-quality spectra were obtained with all four channels in 2000 July. By design, most wavelengths in the *FUSE* bandpass are recorded by at least two channels (see Figure 3 in Sahnou et al. 2000).

The initial (1999) observations were reduced as described in Oegerle et al. (2000). The later observations were reduced in a similar fashion with CALFUSE version 1.7.6. The data were recorded in time-tag mode and were processed to correct for Doppler shifts due to orbital motion, subtract backgrounds, and wavelength and flux calibrate the spectra. Flatfield and astigmatism corrections were not sufficiently tested at the time of processing and were not applied. CALFUSE assumes that the background is uniform across a given detector, which is an adequate approximation for an object as bright as H1821+643. Oegerle et al. (2000) report that the resolution of the 1999 October spectrum is 20–25 km s⁻¹. The resolution of later observations are somewhat better; the FUSE PI Team finds that the current resolution ranges from ~17 to 25 km s⁻¹ (e.g., Savage et al. 2001). In both cases the resolution depends on the wavelength and channel used to record the data. Because of the varying resolution of data from different channels and observation dates, there are differing views on how to best make use of multiple detections of a particular line. We discuss our strategy regarding this issue in §3.

While the wavelength scale of the 1999 October data can show large errors (10–30 km s⁻¹) over small intervals, this problem was subsequently corrected and is not evident in the 2000 July data. The relative dispersion solution of the 2000 July data is accurate to ~6 km s⁻¹. However, there can still be an error in the zero point of the wavelength scale, e. g., due to imperfect centering of the target in the aperture. To set the zero point of the *FUSE* data, the multicomponent Milky Way Fe II λ 1144.9 line was compared to the Galactic Fe II 1608.5 line recorded in the STIS E140M spectrum. Similarly, Lyman series lines in the *FUSE* spectrum at $z_{\text{abs}} = 0.225$, which show distinctive component structure, were compared to the Ly γ line at this redshift in the STIS spectrum. As in Oegerle et al. (2000), the wavelength scale of the 1999 October data was corrected on a line-by-line basis by comparison to appropriate analogous lines in the STIS E140M observation.

3. Absorption Line Measurements

The absorption profiles of detected lines at $z_{\text{abs}} = 0.1212$ as well as regions of undetected species of interest are shown in Figure 1. Standard processing of *FUSE* data provides highly oversampled spectra, so we have rebinned the *FUSE* data to ≈ 7 km s⁻¹ pixels. The STIS data are optimally sampled, so no rebinning has been applied. Remarkably, despite the close proximity of several galaxies (see §1) and a relatively strong Ly α line, only Ly α , Ly β , and the O VI λ 1032 transitions are clearly detected at the

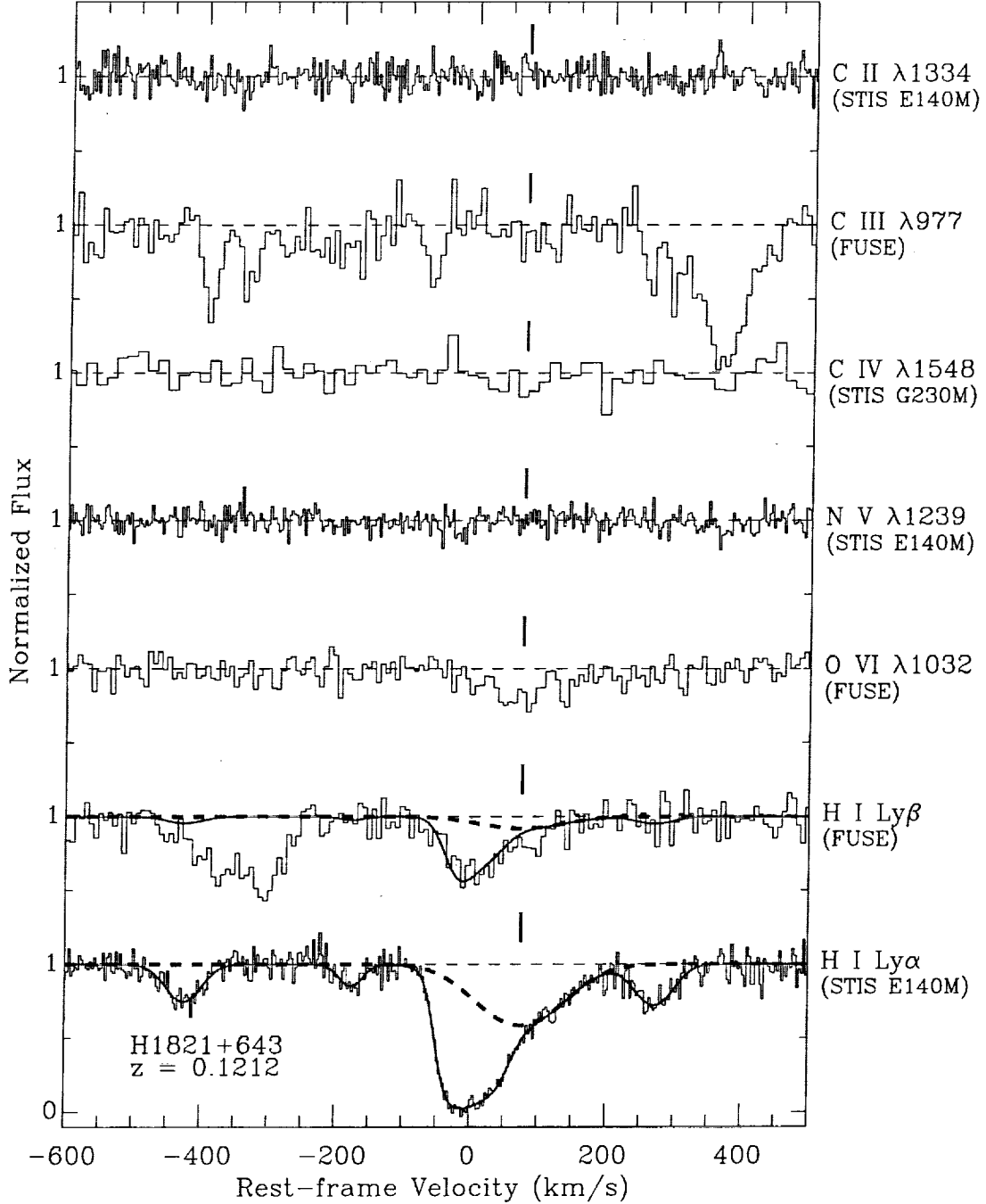


Fig. 1.— Continuum-normalized absorption profiles of the H I Ly α , Ly β , and O VI $\lambda 1032$ lines detected at $z_{\text{abs}} = 0.1212$ in the spectrum of H1821+643 (lower three profiles); the profiles are plotted vs. rest-frame velocity where $v = 0$ at $z_{\text{abs}} = 0.1212$. The C II $\lambda 1334.5$, C III $\lambda 977.0$, C IV $\lambda 1548.2$, and N V $\lambda 1238.8$ lines are not significantly detected at this redshift, and the spectral regions of these undetected lines are shown in the upper portion of the figure. The profile fit which yields the component parameters in Table 2 is overplotted on the Ly α and Ly β profiles with a solid line, and the broad H I component discussed in §4 is shown with a dashed line. For reference, the velocity centroid of this broad component is indicated with a tick mark above each profile. Note that there are several unrelated lines near the C III and Ly β profiles.

4σ level or better at this redshift (we argue below that there is evidence of O VI $\lambda 1038$ absorption as well, although the transition is blended with an unrelated line). Table 1 lists rest-frame equivalent widths (W_r) of the detected absorption lines at $z_{\text{abs}} = 0.1212$, measured using the methods of Sembach & Savage (1992), as well as 4σ upper limits on undetected lines. Note that contributions due to the uncertainty in the curvature and height of the continuum as well as a 2% uncertainty in the flux zero point are included with the statistical uncertainties in the overall errors in Table 1. Integrated apparent column densities (Savage & Sembach 1991), which similarly include continuum placement and zero point uncertainties, are also provided in Table 1.

The quantities in Table 1 are integrated over the full velocity range of the main Ly α feature but do not include the three high-velocity weak Ly α lines evident in Figure 1 at $v = -425, -179$, and $+270$ km s $^{-1}$. However, it is obvious from Figure 1 that even the main Ly α feature is composed of at least two substantially blended components. To deblend these components and measure line widths, we have used the Voigt profile-fitting software of Fitzpatrick & Spitzer (1997) to simultaneously fit the Ly α and Ly β profiles. For the STIS echelle data (Ly α), we have accounted for instrumental broadening using the line spread functions from the STIS handbook; for FUSE data (Ly β), we have assumed that the LSF is adequately described by a Gaussian with FWHM ≈ 20 km s $^{-1}$. The profile-fitting results are summarized in Table 2. The final model profile is overplotted on the Ly α and Ly β profiles in Figure 1 with a solid line.

Two comments on the profile-fitting results are in order. First, the Ly β profile shows excess absorption compared to the model profile over several pixels at $v \approx 90$ km s $^{-1}$. This is due to noise. Since the Ly α f -value is a factor of 5 greater than the Ly β f -value, and since the equivalent width goes as $f\lambda^2$, this “component” would be very prominent in the Ly α profile if it were real. We have attempted to find a set of components which produce this extra Ly β absorption without violating the constraints set by the Ly α profile, and we have been unsuccessful. Since *FUSE* is known to have complex and substantial fixed-pattern noise (Sahnow et al. 2000), it is not too surprising to occasionally encounter a noise feature of this sort. Second, the model profile fitted to the H I lines is not unique. The smoothness of the Ly α profile at $100 \lesssim v \lesssim 200$ km s $^{-1}$ provides some support for fitting this wing with a single broad component, but a comparably good fit can be obtained with several narrower components spread over this velocity range.

In the case of the *FUSE* data, we are primarily interested in *total* equivalent widths and column densities integrated across the full velocity range of the main absorption feature (i.e., $-110 \leq v \leq +210$ km s $^{-1}$ in Figure 1). Given the breadth of the absorption features of interest and the moderate differences in resolution of the various data, it is reasonable to coadd the various spectra to increase the S/N. Nevertheless, to be conservative we have measured integrated equivalent widths and apparent column densities from the individual spectra separately, then we have determined the mean of the individual measurements, each weighted inversely by its variance. These weighted means are the final integrated quantities reported in Table 1. For profile fitting, on the other hand, we fitted the STIS Ly α and *FUSE* Ly β profiles simultaneously. Consequently, to make full use of the *FUSE* observations, we first coadded Ly β profiles with the usual weighting based on the inverse variances of the individual spectra. We similarly coadded the *FUSE* O VI data for the purposes of the next paragraph. Note that Figure 1 shows these coadded Ly β and O VI profiles. Since the Ly β lines are detected at high significance in the individual spectra, we elected to coadd only the Ly β profiles from the two LiF channels obtained in 2000 July and thereby preserve the resolution as much as possible. However, the O VI lines are detected at lower significance in the individual channels, and one of the LiF channels from 2000 July is not useful in the O VI region due to the vertical stray light stripe caused by scattered terrestrial Ly α emission during spacecraft orbital daytime (see §2.3 in Sahnow et al. 2000). Consequently, for the O VI lines we have coadded both of the LiF channels from

Table 1. Equivalent Widths and Integrated Column Densities of the O VI Absorber at $z = 0.1212$

Species	λ_0^a (Å)	f^a	W_r^b (mÅ)	$\log N_a^c$	Spectrograph
H I.....	1215.67	0.416	595 ± 12	$>14.38^d$	STIS E140M
H I.....	1025.72	0.0791	158 ± 14	14.43 ± 0.04	FUSE ^e
O VI.....	1031.93	0.133	90 ± 17	14.02 ± 0.07	FUSE ^f
N V.....	1238.82	0.156	$<56^g$	$<13.42^g$	STIS E140M
C IV.....	1548.20	0.191	$<144^g$	$<13.55^g$	STIS G230M
C III.....	977.02	0.759	$<104^g$	$<13.21^g$	FUSE ^h
C II.....	1334.53	0.127	$<62^g$	$<13.49^g$	STIS E140M
Si IV.....	1393.76	0.514	$<55^g$	$<12.79^g$	STIS E140M
Si III.....	1206.50	1.669	$<70^g$	$<12.51^g$	STIS E140M

^aRest frame vacuum wavelength and oscillator strength from Morton (2001) or Morton (1991).

^bRest frame equivalent width integrated from -110 to 210 km s^{-1} where $v = 0 \text{ km s}^{-1}$ at $z_{\text{abs}} = 0.1212$.

^cApparent column density integrated from -110 to 210 km s^{-1} . For undetected lines, 4σ upper limits are derived from the upper limits on W_r using the linear portion of the curve of growth.

^dSaturated absorption line.

^eWeighted mean of individual measurements from the observations with the LiF1b and LiF2a detectors on 1999 October 17 and 2000 July 24.

^fWeighted mean of individual measurements from the observations with the LiF1b and LiF2a detectors on 1999 October 17 and the LiF2a detector on 2000 July 24. The LiF1b spectrum from 2000 July 24 was adversely affected by the vertical stray light “stripe” (Sahnou et al. 2000) and is too noisy to provide a useful measurement.

^g 4σ upper limit.

^hBased on the LiF2a spectrum from 2000 July 24 only.

Table 2. Component Parameters of the Ly α and Ly β Absorption Lines at $z = 0.1212^a$

Redshift ^b	v^c	b (km s ⁻¹)	$\log N$
0.11961	-425	35 \pm 9	13.14 \pm 0.04
0.12053	-179	23 $^{+15}_{-9}$	12.71 \pm 0.08
0.12112	-21	26 $^{+13}_{-9}$	13.93 \pm 0.37
0.12125	13	40 $^{+44}_{-21}$	14.04 \pm 0.36
0.12147	72	85 $^{+37}_{-26}$	13.78 \pm 0.17
0.12221	270	38 \pm 9	13.22 \pm 0.04

^aBased on simultaneous profile fitting of the Ly α and Ly β lines with the software of Fitzpatrick & Spitzer (1997) and the STIS E140M line spread functions from the STIS Instrument Handbook. The FUSE LSF was taken to be a Gaussian with FWHM ≈ 20 km s⁻¹.

^bHeliocentric redshift; the conversion from a heliocentric velocity scale to the Local Standard of Rest velocity scale is given by $v_{\text{LSR}} = v_{\text{helio}} + 16$ km s⁻¹ assuming the Sun is moving in the direction $l = 56^\circ, b = 23^\circ$ at 19.5 km s⁻¹ (Kerr & Lynden-Bell 1986).

^cComponent velocity centroid in the rest frame of the absorption system where $v = 0$ km s⁻¹ at $z_{\text{abs}} = 0.1212$.

the 1999 observations with the one useful LiF channel (LiF2) from the 2000 observations. We note that the measurements from the individual channels are consistent within their 1σ uncertainties.

Since O VI has a resonance-line doublet, its absorption lines can usually be unambiguously identified. Unfortunately, the weaker 1038 Å line of the O VI doublet at $z_{\text{abs}} = 0.1212$ in the spectrum of H1821+643 is strongly blended with the Ly δ line from the absorption system at $z_{\text{abs}} = 0.225$, which may lead some readers to question the reliability of the identification of the stronger O VI $\lambda 1032$ line shown in Figure 1. However, since the Ly δ line is not strongly saturated, we should be able to demonstrate that the 1038 Å line is present if the S/N is sufficient, and indeed we do find evidence of the 1038 Å line at the expected wavelength and strength. Figure 2 shows this evidence. This figure shows the continuum-normalized, coadded O VI profiles. A single-component fit to the O VI $\lambda 1032$ line *only* is shown with a dashed line overplotted on the 1032 Å profile (upper histogram). The velocity, column density, and Doppler parameter from this fit predict a 1038 Å absorption line shown with a dashed line shown overplotted on the lower histogram in Figure 2. Absorption is clearly present in the lower profile at the expected velocity with the expected strength. This gives us confidence that the O VI identification is correct.

4. Physical Conditions and Metallicity

In this section we explore the implications of the absorption-line measurements regarding the ionization and metallicity of the gas. We first consider collisional ionization, and then we examine photoionization. Before assessing the ionization mechanism, we comment on several interesting features of this absorber:

1. The O VI absorption occurs at a redshift where there is a cluster of Ly α absorption lines; at least five Ly α lines are present within a velocity interval of $\sim 700 \text{ km s}^{-1}$ (see Figures 1 and 3).
2. Furthermore, there are several galaxies within $\pm 500 \text{ km s}^{-1}$ of this redshift with projected distances from the sight line ranging from $144 h_{75}^{-1} \text{ kpc}$ to 3.1 Mpc (see Tripp et al. 1998). Figure 3 shows the velocities and projected distances of these galaxies with respect to the Ly α absorption lines [Tripp et al. (1998) estimate that the galaxy redshift uncertainties are $\sim 50 - 100 \text{ km s}^{-1}$]. As noted in §1, the closest galaxy has an emission line spectrum which suggests that it is actively forming stars.
3. In addition to an ordinary, mildly saturated narrow line, the main Ly α profile appears to contain a relatively broad component at $v = 72 \text{ km s}^{-1}$ with $b \approx 85 \text{ km s}^{-1}$ (see Table 2; this broad component is shown with a heavy dashed line in Figure 1). This implies an upper limit on the temperature of the gas at this v : $T \leq mb^2/2k = 4.3 \times 10^5 \text{ K}$. Therefore this absorption could arise in the warm/hot, shock-heated phase predicted by cosmological simulations. This is an upper limit because the profile could be broadened by factors other than thermal motions such as turbulence, multiple blended components, or expansion of the Universe. If the broadening is predominantly due to cosmological expansion, then the implied pathlength l through the absorber is given by $\Delta v \approx 15.0 \text{ km s}^{-1} (l/200 \text{ kpc})h_{75}$. Taking $\Delta v \approx \text{FWHM} = 142 \text{ km s}^{-1}$ for the broad H I component, we obtain $l \lesssim 1.9 h_{75}^{-1} \text{ Mpc}$ in this case.
4. The O VI absorption is not aligned with the strongest portion of the H I profile (i.e., the saturated component at $v \approx 0 \text{ km s}^{-1}$). Rather, the O VI is reasonably well-aligned with the broad H I component at $v = 72 \text{ km s}^{-1}$.⁹ The O VI line is also apparently broad; the profile fit shown in Figure 2

⁹Oegerle et al. (2000) suggested that the H I Ly β and O VI centroids were offset but could not be sure of the magnitude of

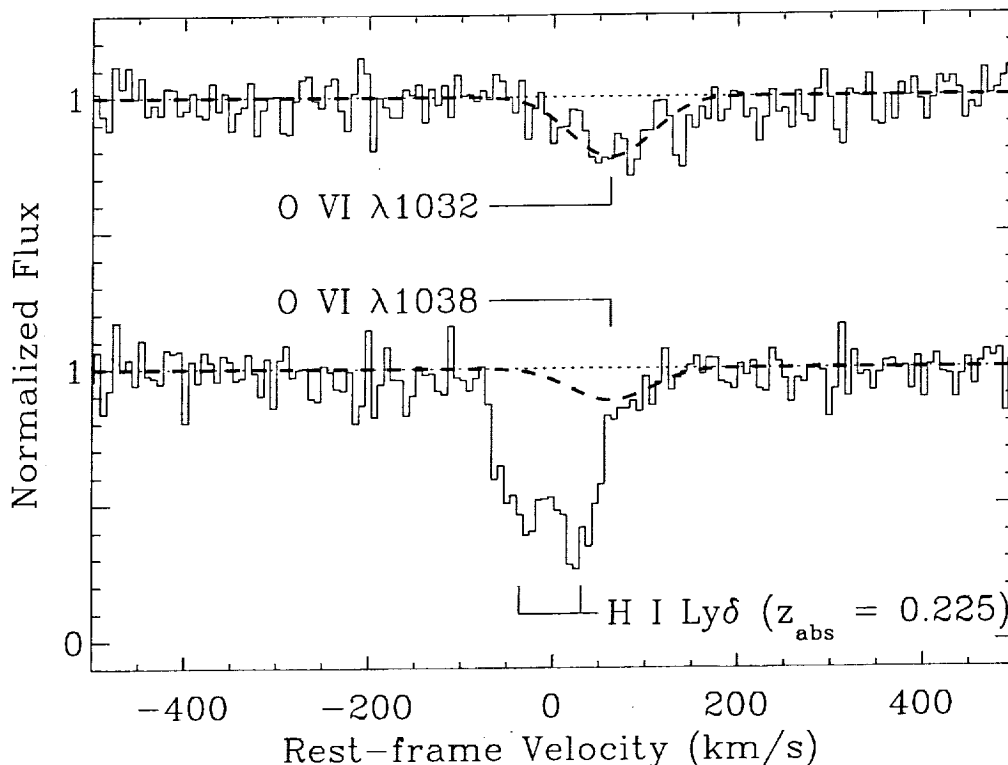


Fig. 2.— Continuum-normalized absorption profile of the O VI $\lambda 1032$ line at $z_{\text{abs}} = 0.1212$ (upper histogram), and the spectral region where the corresponding O VI $\lambda 1038$ line is expected (lower histogram), both plotted versus rest-frame velocity where $v = 0 \text{ km s}^{-1}$ at $z_{\text{abs}} = 0.1212$. Both profiles are derived from the coadded data from different channels and observation dates (see text). The O VI $\lambda 1038$ line is strongly blended with a Ly δ line at $z_{\text{abs}} = 0.225$. Nevertheless, there is evidence that the O VI $\lambda 1038$ line is present. The dashed line overplotted on the $\lambda 1032$ profile shows the result of a single-component fit to the 1032 Å line *only*. The velocity, Doppler parameter, and column density from this fit were used to predict the strength of the corresponding (blended) $\lambda 1038$ transition, and the predicted 1038 Å line is overplotted with a dashed line on the lower profile. An absorption feature with the predicted velocity, strength, and width is readily apparent.

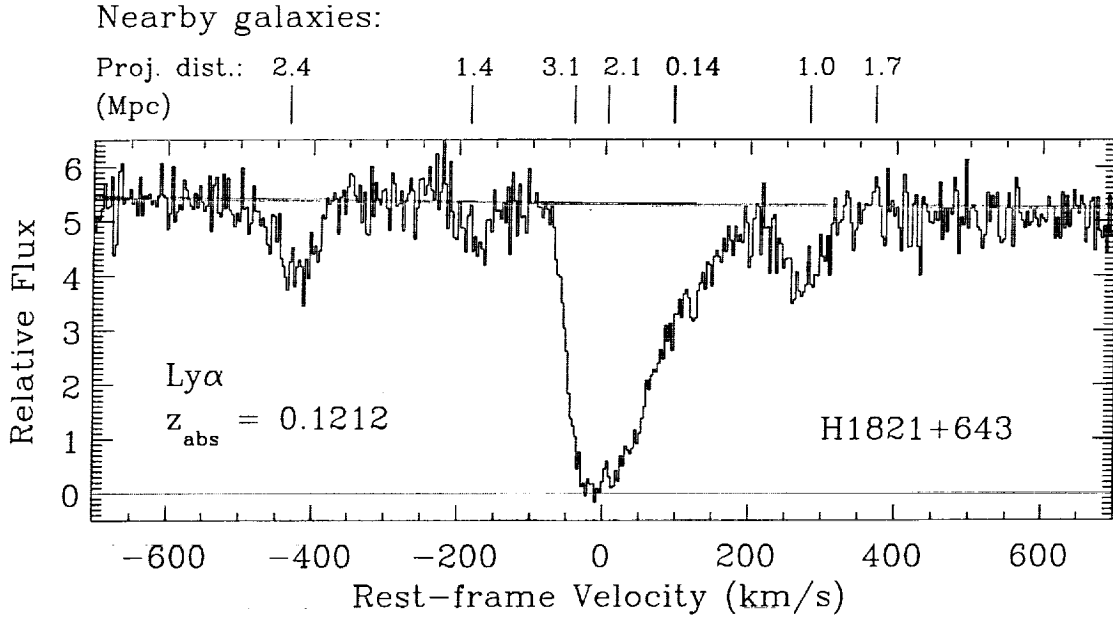


Fig. 3.— Cluster of Ly α absorption lines near the redshift of the O VI absorber at $z_{\text{abs}} = 0.1212$. The relative (unnormalized) flux is plotted versus rest-frame velocity where $v = 0 \text{ km s}^{-1}$ at $z_{\text{abs}} = 0.1212$, and the continuum placement used for the measurements in Tables 1 and 2 is shown with a solid gray line. Seven galaxies with measured redshifts are close to the line of sight at $z \approx 0.1212$; their velocities in this frame [$\Delta v = c\Delta z/(1+z)$] are indicated with tick marks at the top of the panel, and the numbers above each tick indicate the projected distance of the galaxy from the sight line. The uncertainties in the galaxy redshifts are estimated to be $50\text{--}100 \text{ km s}^{-1}$.

has $b = 59^{+30}_{-20}$ km s⁻¹. This would imply a high temperature if entirely due to thermal motions and may be evidence of another source of broadening (see below). The upper limit on the temperature of the O VI gas for $b = 59$ km s⁻¹ is $T \leq 3.3 \times 10^6$ K.

5. As noted above, no metals apart from O VI are significantly detected despite coverage of very strong resonance transitions of abundant elements (e.g., C II $\lambda 1334$, C III $\lambda 977$, and Si III $\lambda 1206$). There is a marginal feature near the expected wavelength of C IV $\lambda 1548$ (see Figure 1), but its significance is less than 3σ and no feature is evident at the expected wavelength of C IV $\lambda 1550$. Consequently, we use the 4σ upper limit on C IV for all purposes of this paper, and we obtain $N(\text{O VI})/N(\text{C IV}) \geq 3.0$.

4.1. Collisional Ionization

Can collisional ionization produce the observed properties of this O VI absorber? In collisionally ionized gas in equilibrium (we briefly discuss non-equilibrium models at the end of §4.2), the O VI ionization fraction is maximized at $T \approx 300,000$ K (Sutherland & Dopita 1993). The H I ion fraction is small at such temperatures, but nevertheless, by virtue of the great abundance of hydrogen, H I Ly α absorption associated with hot O VI should be detectable. Therefore H I absorption lines which are rather broad due to thermal motions are expected to arise in the warm/hot IGM discussed by Cen & Ostriker (1999a), and the broad H I and O VI lines shown in Figure 1 seem to provide promising evidence for the warm/hot gas. Does this hold up under scrutiny? The temperature implied by the apparent breadth of the H I component aligned with the O VI is about right for collisional ionization. The lower limit on the O VI/C IV ratio provides a lower limit on the temperature: assuming the gas is in equilibrium, we find from the calculations of Sutherland & Dopita (1993) that $N(\text{O VI})/N(\text{C IV}) \geq 3.0$ requires $T \geq 10^{5.3}$ K. Combined with the temperature upper limit from the broad H I component, we have $10^{5.3} \leq T \leq 10^{5.6}$ K.

As noted above, the single-component O VI fit shown in Figure 2 implies $T \leq 3.3 \times 10^6$ K. While it is possible to detect trace O VI absorption in gas with $T \gtrsim 10^6$ K, the corresponding H I absorption would be quite broad and inconsistent with the observed Ly α profile. It seems more likely that the O VI is at least partially broadened by non-thermal motions or multiple components. This non-thermal broadening would affect associated H I as well but would not preclude substantial thermal broadening in the H I profile. For example, if we assume that the broad H I and O VI absorption lines arise in the same gas and that the non-thermal motions can be adequately described by a Gaussian profile, then we can express the b -value as $b^2 = b_{\text{nt}}^2 + 2kT/m$ and solve for T and b_{nt} , the contribution from non-thermal motions. With $b(\text{H I}) = 85$ km s⁻¹ and $b(\text{O VI}) = 59$ km s⁻¹, we obtain in this way $T = 2.4 \times 10^5$ K and $b_{\text{nt}} = 57$ km s⁻¹.

The ionization mechanism can also be usefully tested by considering the metallicity required by the model – a model which requires an excessively high metallicity may be unrealistic. We estimate the gas metallicity as follows. Using the usual logarithmic notation, $[\text{O}/\text{H}] = \log(\text{O}/\text{H}) - \log(\text{O}/\text{H})_{\odot}$, the oxygen abundance can be expressed as

$$\left[\frac{\text{O}}{\text{H}}\right] = \log\left(\frac{N(\text{O VI})}{N(\text{H I})}\right) + \log\left(\frac{f(\text{H I})}{f(\text{O VI})}\right) - \log\left(\frac{\text{O}}{\text{H}}\right)_{\odot} \quad (1)$$

the offset because of problems with the wavelength scale in the early *FUSE* data. These problems have been rectified, and the offset is now reliably determined.

where f is the ion fraction and $(\text{O}/\text{H})_{\odot}$ is the solar oxygen abundance.¹⁰ Since $N(\text{O VI})$ and $N(\text{H I})$ are measured quantities and $(\text{O}/\text{H})_{\odot}$ is fixed, $[\text{O}/\text{H}]$ can be estimated by using an ionization model to estimate $f(\text{H I})/f(\text{O VI})$.

Assuming the broad H I component shown in Figure 1 originates in the same gas as the O VI absorption, we have $\log N(\text{H I}) = 13.78$ and $\log N(\text{O VI}) = 14.02$ from Tables 1 and 2. Then, taking $f(\text{H I})/f(\text{O VI})$ vs. T from Sutherland & Dopita (1993), we derive from equation 1 the oxygen abundance as a function of T required to match the measured $N(\text{H I})$ and $N(\text{O VI})$. This is shown in Figure 4. The lower limit on the temperature from $N(\text{O VI})/N(\text{C IV})$ and the upper limit on T from the H I line width are also indicated in Figure 4; the hatched gray regions are not consistent with these constraints. From this figure, we see that within the temperature limits, the observed column densities can be reproduced in gas with $-1.8 \lesssim [\text{O}/\text{H}] \lesssim -0.6$, i.e., 0.02 – 0.25 solar metallicity.

This allowed range of metallicities is in reasonable agreement with theoretical expectations for intergalactic gas. For example, the study of IGM metal enrichment by Cen & Ostriker (1999b) indicates that this range of metallicity could arise in regions with a wide range of overdensity $\delta = \rho / \langle \rho \rangle$ (see the $z = 0$ curve in their Figure 2), and $Z \sim 0.1 Z_{\odot}$ would not be surprising given the H I column density of the absorber studied here. The models of Aguirre et al. (2001), which use various semi-analytic prescriptions to explore how metals might be distributed within a previously computed hydrodynamic simulation, predict somewhat lower mean metallicities at $z = 0$. The mean metallicity is somewhat less than 0.02 solar for $\delta < 100$ in their supernova-driven wind models, for example. However, their calculation only includes enrichment from galaxies with baryonic mass $> 3 \times 10^{10} M_{\odot}$, and inclusion of smaller galaxies could increase the metallicity by a factor of a few. Furthermore, since this is a mean metallicity, there are certainly higher metallicity regions in the models, and some of these are likely to be consistent with the requirements derived above for the $z_{\text{abs}} = 0.1212$ absorber. Of course, it is possible that this absorber does not originate in a particularly low overdensity region – the presence of several galaxies close to the absorber redshift suggests that this absorber may be due to gas within a galaxy group, or at least a somewhat overdense filament. However, the metallicity range shown in Figure 4 is reasonable in this scenario as well: X-ray observations (e.g., Davis, Mulchaey, & Mushotzky 1999; Hwang et al. 1999) of galaxy groups indicate that the intragroup medium metallicity is consistent with the upper portion of the range derived for this absorber.

The H I and O VI absorption line kinematics are intriguing in the context of collisional ionization. The juxtaposition of a relatively narrow H I component at $v \approx 0 \text{ km s}^{-1}$ with a broad H I + O VI component separated by $\sim 75 \text{ km s}^{-1}$ is suggestive of shock-heating in two colliding clouds, with the O VI and broad H I arising in the post-shock gas. If we estimate the shock velocity by scaling the apparent velocity separation of the components by $\sqrt{3}$ (to account for projection effects), we estimate that two clouds colliding at a velocity $v_s = \sqrt{3} \times 75 \text{ km s}^{-1} = 130 \text{ km s}^{-1}$ would be shock-heated to $T \approx 2.3 \times 10^5 \text{ K}$, assuming a standard shock¹¹ with specific heat ratio $\gamma = 5/3$. This temperature, shown with a vertical dotted line in Figure 4, is consistent with the temperature constraints derived above.¹²

¹⁰Throughout this paper we adopt the solar abundances reported by Grevesse & Anders (1989) and Grevesse & Noels (1993). These reference abundances have been widely used in recent literature. However, use of the recent revisions of the solar oxygen abundance (Holweger 2001; Allende Prieto et al. 2001; see also Sofia & Meyer 2001) increases $[\text{O}/\text{H}]$ by $\sim 0.1 - 0.2 \text{ dex}$.

¹¹For a standard shock with $\gamma = 5/3$, the mean post-shock temperature is given by $T_s = 1.38 \times 10^5 (v_s/100 \text{ km s}^{-1})^2 \text{ K}$ (see, e. g., McKee & Hollenbach 1980; Draine & McKee 1993).

¹²If the scale factor to correct for projection effects is less than $\sqrt{3}$, then T_s could drop below the lower limit on the gas temperature set by $N(\text{O VI})/N(\text{C IV})$. However, the component of the shock velocity which is projected onto the line-of-sight

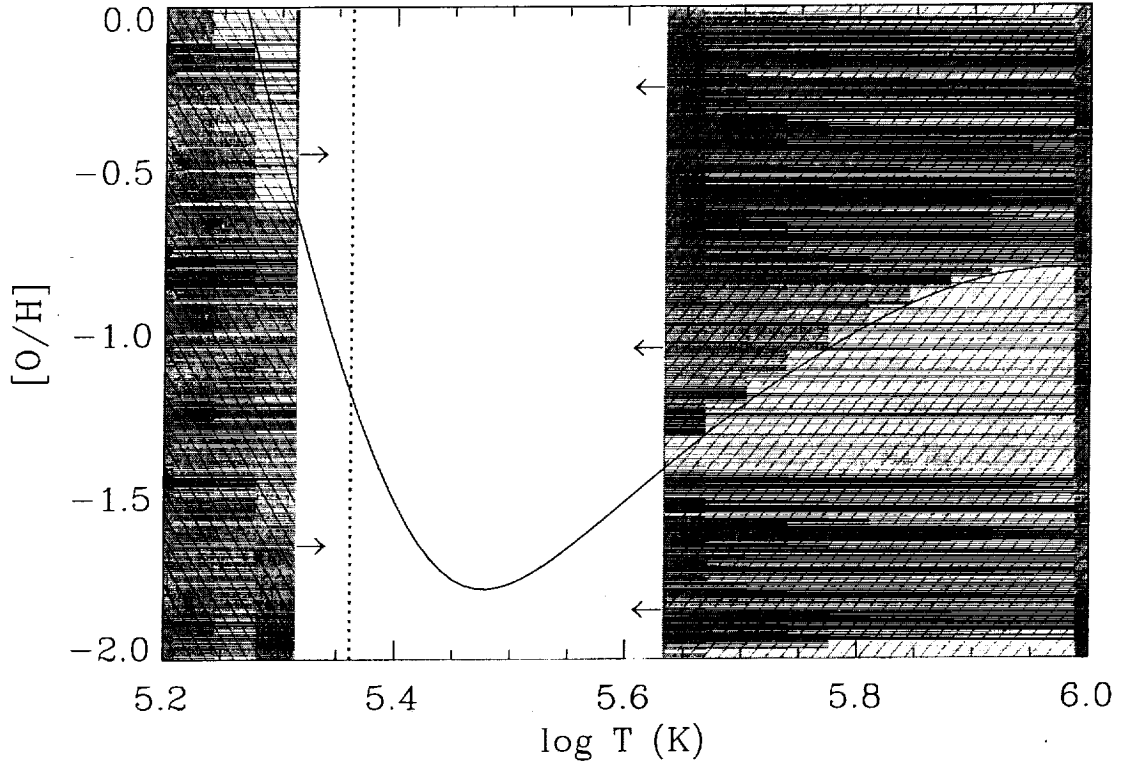


Fig. 4.— The logarithmic oxygen abundance $[O/H]$ required to produce the observed O VI and H I column densities *in the broad component* of the absorber at $z_{\text{abs}} = 0.1212$, assuming the gas is collisionally ionized and in equilibrium, as a function of temperature (solid line). This follows from the O VI and H I ionization fractions vs. T (from Sutherland & Dopita 1993) and equation 1. The gray regions of the plot indicate regions which are not allowed by other constraints; the lower limit on T is set by the lower limit on $N(\text{O VI})/N(\text{C IV})$, and the upper limit on T is set by the b -value of the broad H I component associated with the O VI absorption. The vertical dotted line indicates the mean post-shock temperature for a standard shock with $v_s = 130 \text{ km s}^{-1}$.

Summarizing this section, we find that the observed properties of this absorber can be produced by collisionally ionized gas in equilibrium with $5.3 \leq \log T \leq 5.6$ and $-1.8 \leq [\text{O}/\text{H}] \leq -0.6$. These properties are consistent with expectations for the IGM as well as the intragroup medium in galaxy groups. Equilibrium collisional ionization is evidently a viable ionization mechanism for this absorber.

4.2. Photoionization

Is photoionization also viable for this absorber? To address this question we have constructed standard models with the photoionization code CLOUDY (Ferland et al. 1998). The models adopt the usual assumptions: the absorber has constant density and the geometry is plane-parallel, the gas is photoionized by the UV background from QSOs and AGNs at $z \approx 0.12$ as calculated by Haardt & Madau (1996),¹³ and the mean intensity at 1 Rydberg is set to $J_\nu(\text{LL}) = 1 \times 10^{-23} \text{ ergs s}^{-1} \text{ cm}^{-2} \text{ Hz}^{-1} \text{ sr}^{-1}$, a value in reasonable agreement with observations (e.g., Kulkarni & Fall 1993; Maloney 1993; Vogel et al. 1995; Donahue, Aldering, & Stocke 1995; Tumlinson et al. 1999; Davé & Tripp 2001) and theoretical predictions (e.g., Haardt & Madau 1996; Fardal, Giroux, & Shull 1998; Davé et al. 1999; Shull et al. 1999b). With these assumptions, we varied the gas metallicity and ionization parameter U ($= n_\gamma/n_{\text{H}} = \text{ionizing photon density/total hydrogen number density}$) to find the parameter ranges consistent with the observed O VI and H I column densities in the broad component and the upper limits in Table 1. Note that since $J_\nu(\text{LL})$ is fixed at an assumed value, varying U is tantamount to varying n_{H} . Since the photoionization model computes the H ion fraction, once U is constrained, the total H column density and thickness (or pathlength) of the absorber are also constrained.

The results of the photoionization models are shown in Figure 5 where we have used the $f(\text{O VI})$ and $f(\text{H I})$ from the photoionization code to derive $[\text{O}/\text{H}]$ vs. $\log U$ using equation 1. From the measurements available in Table 1, we find that the lower limit on $N(\text{O VI})/N(\text{C IV})$ is the most useful for constraining the ionization parameter; from this ratio we derive $\log U \geq -1.20$. A rough upper limit on U is provided by the required pathlength through the absorber. If the pathlength is too large, the lines would be broader than the observed lines due to cosmological expansion. Using the rough upper limit on l derived in §4, we find $\log U \lesssim -0.6$. As before, the gray hatching in Figure 5 indicates regions which are not consistent with these constraints. From this figure, we see that the observational constraints are satisfied if $-1.1 \leq [\text{O}/\text{H}] \lesssim -0.3$ and $85 \leq l \lesssim 1900 \text{ kpc}$. To derive these metallicities, we have assumed $\log N(\text{H I}) = 13.78$ from the broad component fit shown in Figure 1. In the photoionized scenario, the H I Ly α absorption line arising in the O VI gas could be substantially narrower, and this would lead to a lower H I column density. This, in turn, would require an even higher oxygen abundance to produce the observed $N(\text{O VI})$ [see eqn. 1]. However, $\log N(\text{H I}) = 13.78$ is likely a reasonable upper limit in this case, and therefore these models provide lower limits on the metallicity if the gas is photoionized.

The physical properties implied by the photoionization models are reasonable. For example, Schaye (2001) has analytically derived expressions for the density and size of Ly α absorbers, assuming only that the gas is photoionized and in local hydrostatic equilibrium. Using his equations (8) and (12), and assuming the gas temperature $T \sim 10^4 \text{ K}$, the H I photoionization rate $\Gamma \sim 10^{-13.3} \text{ s}^{-1}$, and the fraction of the mass in

could also be larger than 75 km s^{-1} , which would offset this effect. The point here is that the observed absorption lines have approximately the right velocities to produce O VI in a shock.

¹³We have also computed models using the UV background calculated by Shull et al. (1999b), and we obtain very similar results.

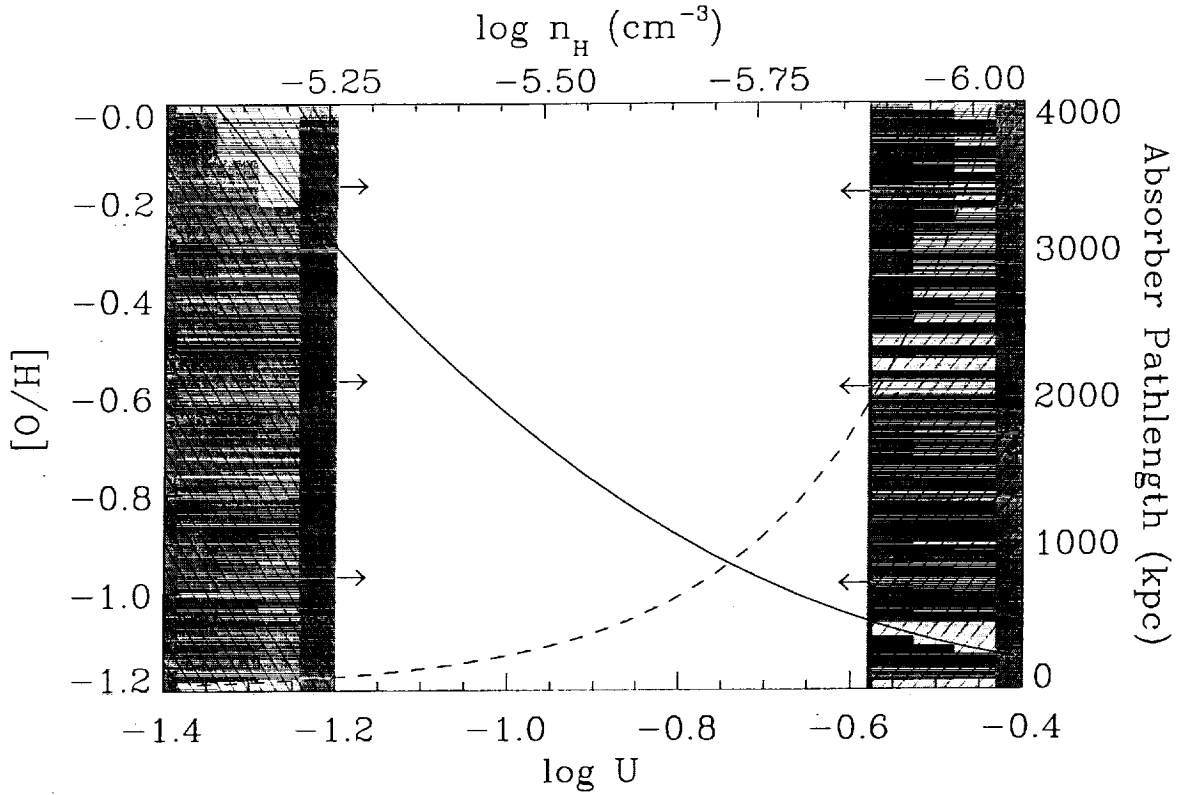


Fig. 5.— The logarithmic oxygen abundance $[O/H]$ (solid line) required to produce the observed O VI and H I column densities *in the broad component* of the absorber at $z_{\text{abs}} = 0.1212$, assuming the gas is photoionized by the UV background from QSOs, as a function of the ionization parameter (bottom axis) and the total H density (top axis) for $J_{\nu}(\text{H I}) = 1 \times 10^{-23} \text{ ergs s}^{-1} \text{ cm}^{-2} \text{ Hz}^{-1} \text{ sr}^{-1}$. The the O VI and H I ionization fractions vs. $\log U$ were calculated with CLOUDY (see text). The dashed line shows the required pathlength through the absorber vs. $\log U$ using the scale on the right axis.

gas $f_g \sim 0.2$, we obtain $\log n_H \lesssim -5.6$ and $l \gtrsim 300$ kpc for $\log N(\text{H I}) \leq 13.78$. These properties are entirely consistent with the properties inferred from the CLOUDY models (see Figure 5). Perhaps the most serious concern about these photoionization models is that the IGM must be substantially and uniformly enriched with metals over a long pathlength. This problem is less severe at higher metallicities because the required pathlengths are smaller. However, the minimum absorber thickness (set by the lower limit on U from O VI/C IV) is 85 kpc for $[\text{O}/\text{H}] = -0.3$. Some QSO absorbers have been observed which apparently have very low metallicities (e.g., Shull et al. 1999a), so the IGM has not been *generally* enriched to this level, but the system of this paper could arise in a more metal-rich region. As noted above, the mean metallicities predicted by simulations (e.g., Cen & Ostriker 1999b; Aguirre et al. 2001) are only marginally consistent with such a high metallicity, but again this could be a particularly high Z region. Cen & Bryan (2001) have argued that most of the metals in the diffuse, low-density intergalactic gas are provided by small galaxies ($M < 10^9 M_\odot$) and are injected into the IGM at $z > 4$. Because larger galaxies which form later do not widely disperse their metals, Cen & Bryan expect that low- z , low column density Ly α clouds will have low metallicities. A similar picture has been favored by Heckman et al. (2000) based on the observed properties of supernova-driven “superwinds” from low- z starburst galaxies and high- z Lyman-break galaxies (Pettini et al. 2001). Heckman et al. argue that metals injected into the IGM via superwinds, primarily from the lower-mass galaxies, could increase the IGM metallicity to $\sim 1/6$ solar metallicity in the intracluster medium as well as the general IGM. However, in most supernova-wind enrichment scenarios, the O VI gas should be predominantly collisionally ionized. Radiation-pressure driven outflows of dust from galaxies (e.g., Aguirre et al. 2001) could transport heavy elements more gently.

It is interesting to note that Savage et al. (2001) have identified an intervening O VI absorber at $z_{\text{abs}} = 0.06807$ in the spectrum of PG0953+415 which is apparently well-explained by photoionization. In this case, H I, C III, C IV, and N V are also detected and are well-aligned with the O VI, and all of the column densities are reasonably matched by a photoionization model, albeit with a somewhat uncomfortably high metallicity/pathlength combination. Perhaps more importantly, the H I Ly α and Ly β lines associated with the O VI are narrow and appear to be composed of only one component, and the upper limit on T from the width of the H I lines is $T \leq 4.1 \times 10^4$ K. This precludes collisional ionization, at least in equilibrium, unless the H I arises in a different phase from the O VI. A similar situation is found for the O VI system studied by Tripp & Savage (2000), although in this case it is possible to hide a broad component in the complicated Ly α profile, assuming the absorber is a multiphase medium (see their Figure 6). While these examples would seem to strongly favor photoionization, it is also possible that they represent cases where the gas was shock-heated to $\sim 10^6$ K and then cooled more rapidly than it could recombine, as discussed by various authors (e.g., Edgar & Chevalier 1986). Table 4 in Tripp & Savage (2000) summarizes high ion ratios predicted by four non-equilibrium collisional ionization models. Comparison of the high ion column densities measured in this paper to that table shows that most non-equilibrium collisional ionization models satisfy the observational constraints. Of course, in this hypothesis, the substantial breadth of the H I profile would be unexpected, and some other broadening mechanism would need to be invoked. This could simply be the kinematics of the gas, e.g., in a galactic wind.

4.3. X-ray Absorption Lines

In principle, one promising means to break the collisional ionization/photoionization degeneracy is to search for X-ray absorption lines, primarily the resonance transitions of O VII and O VIII at 574 eV and 654 eV, respectively (21.6 and 19.0 Å). Several groups have discussed various aspects of the use of

these lines and their detection with current X-ray facilities (Shapiro & Bahcall 1980; Aldcroft et al. (1994); Hellsten, Gnedin, & Miralda-Escudé 1998; Perna & Loeb 1998; Fang & Canizares 2000; Fang et al. 2001). A complete summary of this literature is beyond the scope of this paper, but we note that the first attempt to *detect* these absorption lines in the diffuse IGM (with the *Chandra* High Energy Transmission Grating Spectrometer) has yielded upper limits of $N(\text{O VIII}) \lesssim 10^{17} \text{ cm}^{-2}$ (Fang et al. 2001).

Given this rough guideline for detection capabilities with current X-ray telescopes, can we hope to determine the ionization mechanism of these O VI absorbers by searching for the corresponding X-ray absorption lines at the same redshifts? To explore this question, we show the O VI/O VII, O VI/O VIII, and O VII/O VIII column density ratios predicted for collisionally ionized gas (in equilibrium) and photoionized gas in Figures 6a and 6b, respectively, for the expected ranges of T and U . The ratios for collisionally ionized gas are based on the calculations of Sutherland & Dopita (1993). The ratios for photoionized gas are from the CLOUDY models described in §4.2. Equilibrium collisional ionization and photoionization clearly have different signatures in these ratios. For example, the O VI/O VII ratio has a much broader range in collisionally ionized gas than in photoionized gas: given the temperature and ionization parameter constraints derived in §4 for the particular absorber of this paper, the models predict $-1 \lesssim \log(\text{O VI/O VII}) \lesssim 1$ for collisionally ionized gas and $\log(\text{O VI/O VII}) \approx 0$ for photoionized gas. Furthermore, if $\log(\text{O VI/O VII}) \approx 0$, then the O VIII line can distinguish between the two models because in this situation the O VI/O VIII ratio is much larger in the collisionally ionized model than the photoionized model.¹⁴ While Figure 6 demonstrates the potential of X-ray observations, it unfortunately also shows that for the O VI system studied here, the O VII and O VIII lines are predicted to have column densities well below 10^{17} cm^{-2} and therefore may be difficult or impossible to detect with current instruments. X-ray observations of other absorbers with larger O VI column densities may be more illuminating. However, if the O VI column density is too much larger, then the O VI lines will saturate making $N(\text{O VI})$ difficult to reliably measure. It seems that it will be difficult to study O VI, O VII, and O VIII absorption arising from the same gas. If the higher oxygen ions were detected at the redshift of one of the H1821+643 O VI systems, this would likely indicate the presence of multiphase gas with the O VII and O VIII revealing a more highly ionized phase containing little O VI.

This discussion has several caveats. First, we have assumed that either collisional ionization or photoionization dominates. In fact, both ionization mechanisms may contribute. Hellsten et al. (1998) argue that photoionization by the X-ray background dominates in the production of O VII and O VIII, even if the gas has a temperature of $10^5 - 10^7 \text{ K}$, but this depends on the density of the gas. The O VI might also be produced by the combined effects of collisional and photoionization. Second, the gas is assumed to be in ionization equilibrium. We have already noted that this assumption might not hold for collisionally ionized gas. Photoionized O VI is likely to be in equilibrium, but O VII and O VIII produced by photoionization might be out of equilibrium because the ionization time scales are comparable to the Hubble time (see, e.g., Hellsten et al. 1998). Again, it would be valuable to evaluate the ratios predicted for these ions in non-equilibrium models as well. Finally, the intensity of the X-ray background is uncertain. A full assessment of these issues is beyond the scope of this paper.

¹⁴ Along these lines we note that in general, the O VII and O VIII lines without the O VI constraint may not be able to distinguish between collisional ionization and photoionization because the dotted lines in Figure 6 are degenerate, and the resolution of current X-ray spectrometers is not sufficient to constrain the temperature of the gas based on line widths.

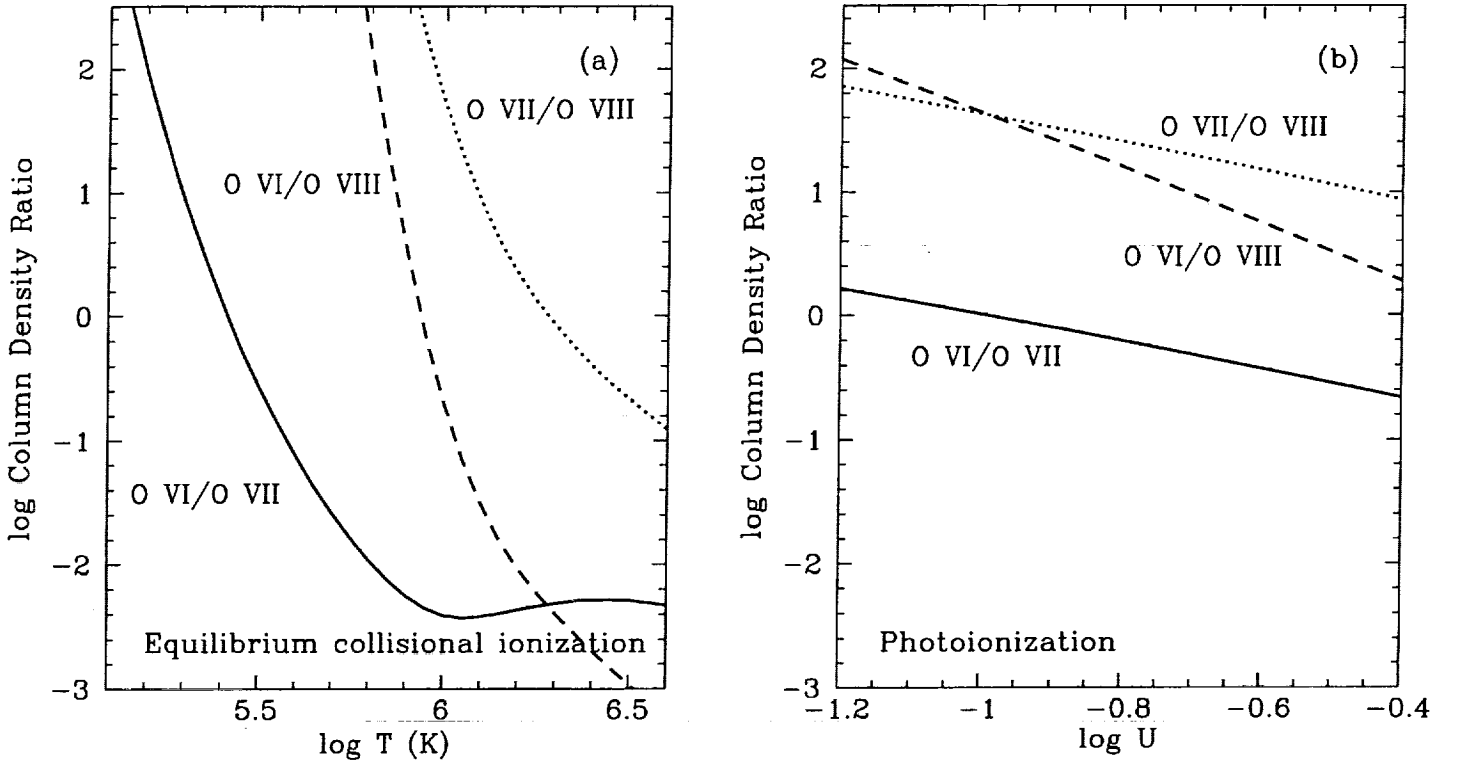


Fig. 6.— Logarithmic column density ratios predicted for O VI/O VII (solid line), O VI/O VIII (dashed line), and O VII/O VIII (dotted line) for (a) collisionally ionized gas in equilibrium, and (b) gas photoionized by the UV background from QSOs. The ratios in the collisionally ionized case are plotted vs. $\log T$, while the photoionized gas ratios are shown vs. \log of the ionization parameter.

5. Summary and Discussion

High-resolution STIS and *FUSE* UV spectra of H1821+643 reveal that the absorption system at $z_{\text{abs}} = 0.1212$ has a number of interesting properties including (1) detection of O VI and H I absorption without significant detection of any other species, (2) complex H I absorption including an apparently broad component with $b \approx 85 \text{ km s}^{-1}$ that is aligned with the O VI absorption, and (3) association with one or more galaxies close to the sight line. Using constraints from these spectra, we have examined the ionization mechanism in this absorber. We find that equilibrium collisional ionization is viable with $5.3 \leq \log T \leq 5.6$ and $-1.8 \leq [\text{O}/\text{H}] \leq -0.6$. However, the absorption line properties can also be explained by photoionization if $-1.1 \leq [\text{O}/\text{H}] \leq -0.3$ and $85 \leq l \lesssim 1900 \text{ kpc}$. In addition, it is possible that the gas is collisionally ionized but is not in equilibrium (e.g., Edgar & Chevalier 1986).

There are a number of possible sites in which O VI absorption lines could arise in the spectra of low- z QSOs. In some cases, O VI absorption likely occurs in the immediate environment of the QSO itself (e.g., Savage et al. 1998; Papovich et al. 2000; Ganguly et al. 2001, and references therein). The large displacement from the QSO redshift and the close association with galaxies near the line of sight indicates that the absorber studied in this paper is *not* in this class. Rather, it is an intervening absorber. However, the detailed nature of the intervening absorption is still unclear – it could occur in the bound ISM of an individual galaxy, the escaping gas in a galactic wind, the intragroup medium of a galaxy group, or a more remote region of a large scale structure or the diffuse IGM.

The galactic wind hypothesis is appealing because O VI absorption has been detected in such an outflow from the nearby starburst galaxy NGC1705 (Heckman et al. 2001). Gas in the temperature range needed to produce O VI by collisional ionization is predicted in hydrodynamic simulations of starburst galaxy winds (e.g., Mac Low & Ferrara 1999; Strickland & Stevens 2000). However, unlike the O VI absorber studied in this paper, the outflow from NGC1705 shows strong absorption lines due to low and intermediate ionization stages as well as O VI. This absorption by low ions is consistent with the hydrodynamic models in which the O VI-bearing gas arises in interfaces between cool, denser gas and much hotter gas (see Figure 4c in Heckman et al. 2001). In this model, low ion absorption occurs in the cool gas, O VI exists in the interface, and the hotter gas produces X-ray emission. The NGC1705 observations probe the ISM and outflow close to the central starburst and its host galaxy, but the $z_{\text{abs}} = 0.1212$ O VI system is at a substantially larger projected distance from any galaxy known to be at the absorber redshift. One could speculate that the character of absorption from a wind is different at larger distances away from the star cluster, but these winds have not been observationally or theoretically studied at such large impact parameters.

The hypothesis that the absorption occurs in the ISM of a galaxy like the Milky Way suffers similar criticisms. While O VI is commonly detected in the disk and halo of the Milky Way (Jenkins 1978; Savage et al. 2000), it would typically be accompanied by absorption from other heavy elements. Galactic high velocity clouds, including clouds stripped out of satellite galaxies, also frequently show associated O VI (Sembach et al. 2000), and high velocity clouds have approximately the same metallicity as the absorber studied in this paper (Wakker et al. 1999; Gibson et al. 2000; Richter et al. 2001). However, a sight line through such an entity would have a much higher H I column density and again would be expected to be detected in other ions.¹⁵

Perhaps the most appealing hypothesis is that the $z_{\text{abs}} = 0.1212$ absorber is due to gas between galaxies

¹⁵The particular absorber studied here is only detected in O VI and H I, but other intervening O VI systems have been detected in other species (Tripp et al. 2000; Chen & Prochaska 2000; Savage et al. 2001).

in a group or unvirialized filamentary structure. Diffuse X-ray emission indicating the presence of a hot intragroup medium has been detected from many galaxy groups (Mulchaey 2000 and references therein), but mainly groups that are elliptical-rich (Mulchaey et al. 1996a; Zabludoff & Mulchaey 1998). Mulchaey et al. (1996b) have suggested that spiral-rich galaxy groups also contain hot intragroup gas, but the gas is not quite hot enough to be detected in X-ray emission ($T \lesssim 4 \times 10^6$ K). They predict that the O VI absorption lines should be detectable in such an intragroup medium. It is interesting that the z_{abs} absorber fits this hypothesis in many respects: (1) there are several galaxies near the sight line at this redshift (see Figure 3), (2) at least one of the galaxies is a spiral/actively star-forming galaxy, and (3) the breadth of the O VI absorption is considerably larger than expected from thermal motions (§4), which is consistent with additional broadening due to the velocity dispersion of the group.¹⁶ However, this may not be a bound group. Given our currently limited information, it is difficult to derive additional information about the collection of galaxies near this O VI absorber, but we do note that the spatial extent of the ensemble appears to be larger than that of a typical poor group (c.f., Zabludoff & Mulchaey 1998). It would be valuable to obtain additional galaxy redshift measurements and high-resolution images for morphological classification.

In §1 we outlined several areas in which additional effort is needed to elucidate the nature of the O VI systems and their contribution to the baryon budget. The main goal of this paper has been to scrutinize the ionization mechanism to test the idea that a substantial quantity of shock-heated hot gas is present in the IGM at the current epoch. We find that the O VI absorber at $z_{\text{abs}} = 0.1212$ in the spectrum of H1821+643 has properties consistent with collisionally ionized hot gas such as a broad H I component aligned with the O VI and a high O VI/C IV ratio. This is encouraging evidence in support of the shock-heated IGM hypothesis. However, we cannot rule out photoionization or a combination of collisional and photoionization processes. The degree of IGM metal enrichment required by photoionization exceeds the predictions of some models, but given our limited understanding of how metals are transported out of galaxies and the variety of possibilities for the absorption site, this is not sufficient grounds to dismiss photoionization. Analyses of other low- z O VI systems (e.g., Tripp & Savage 2000) have reached similar conclusions regarding collisional vs. photoionization.

Given the general difficulty encountered in attempts to definitively identify the ionization mechanism in individual systems, it will be important carry out statistical analyses of O VI absorber samples including comparisons to various models. For example, Cen et al. (2001) and Fang & Bryan (2001) have recently predicted the properties of O VI absorbers based on cosmological simulations. The absorber statistics predicted by these models [e.g., dN/dz and $\Omega_b(\text{O VI})$] appear to be in reasonable agreement with current observations. In these simulations, O VI absorption arises in both collisionally ionized and photoionized gas. However, the photoionized systems are narrower and have lower equivalent widths than the collisionally ionized absorbers. Tripp (2002) has recently presented the b -values and column densities of twenty low- z O VI lines observed with STIS and *FUSE* (see his Figure 5). It is interesting to note that while there are a few apparently narrow O VI lines in the observations compiled by Tripp (2002), the majority of the O VI lines in that sample have b -values consistent with an origin in hot gas. The b -value of an O VI line in gas at $T \sim 300,000$ K is $\sim 18 \text{ km s}^{-1}$, and the median b -value of the observed sample is 22 km s^{-1} . In addition, the apparently narrow O VI lines tend to be weaker systems as well, as predicted by the simulations. These preliminary results appear to be fully consistent with the cosmological simulations. We look forward to similar analyses using larger observational samples and a variety of models.

¹⁶The typical velocity dispersion of a spiral-rich group is $\sim 100 \text{ km s}^{-1}$ (Mulchaey et al. 1996b).

We thank Anthony Aguirre and Joop Schaye for helpful discussions and comments. This research has made use of software developed by the STIS Team for the reduction of STIS data, and we thank the STIS Team for access to this software. The coding of the Robertson optimal extraction was carried out by Bob Hill, and we greatly appreciate this effort. We acknowledge support from NASA through grants GO-08165.01-97A and GO-08182.01-98A from the Space Telescope Science Institute as well as NASA Astrophysical Theory grant NAG5-7262. This work is also based on data obtained for the Guaranteed Time Team by the NASA-CNES-CSA *FUSE* mission operated by the Johns Hopkins University. Financial support to US participants has been provided by NASA contract NAS5-32985.

REFERENCES

- Aguirre, A., Hernquist, L., Schaye, J., Katz, N., Weinberg, D. H., & Gardner, J. 2001, ApJ, in press (astro-ph/0105065)
- Aldcroft, T., Elvis, M., McDowell, J., & Fiore, F. 1994, ApJ, 437, 584
- Allende Prieto, C., Lambert, D. L., & Asplund, M. 2001, ApJ, 556, L63
- Bowen, D. V., Pettini, M., & Boyle, B. J. 1998, MNRAS, 297, 239
- Bowers, C. A., et al. 2001, in preparation
- Brown, T. M., Kimble, R. A., Ferguson, H. C., Gardner, J. P., Collins, N. R., & Hill, R. S. 2000, AJ, 120, 1153
- Burles, S., & Tytler, D. 1998, ApJ, 499, 699
- Cen, R., & Bryan, G. L. 2001, ApJ, 546, L81
- Cen, R., & Ostriker, J. P. 1999a, ApJ, 514, 1
- Cen, R., & Ostriker, J. P. 1999b, ApJ, 519, L109
- Cen, R., Tripp, T. M., Ostriker, J. P., & Jenkins, E. B. 2001, ApJ, in press (astro-ph/0106204)
- Chen, H.-W., & Prochaska, J. X. 2000, ApJ, 543, L9
- Croft, R. A. C., Di Matteo, T., Davé, R., Hernquist, L., Katz, N., Fardal, M. A., & Weinberg, D. H. 2001, ApJ, 557, 67
- Davé, R., Hernquist, L., Katz, N., & Weinberg, D. H. 1999, ApJ, 511, 521
- Davé, R., et al. 2001, ApJ, 552, 473
- Davé, R., & Tripp, T. M. 2001, ApJ, 553, 528
- Davis, D. S., Mulchaey, J. S., & Mushotzky, R. F. 1999, ApJ, 511, 34
- Donahue, M., Aldering, G., & Stocke, J. T. 1995, ApJ, 450, L45
- Draine, B. T., & McKee, C. F. 1993, ARA&A, 31, 373
- Edgar, R. J., & Chevalier, R. A. 1986, ApJ, 310, L27
- Fang, T., & Bryan, G. L., ApJ, submitted
- Fang, T., & Canizares, C. R. 2000, ApJ, 539, 532
- Fang, T., Marshall, H. L., Bryan, G. L., Canizares, C. R. 2001, ApJ, 555, 356
- Fardal, M., Giroux, M. L., & Shull, J. M. 1998, AJ, 115, 2206
- Ferland, G. J., Korista, K. T., Verner, D. A., Ferguson, J. W., Kingdon, J. B., & Verner, E. M. 1998, PASP, 110, 761
- Fitzpatrick, E. L., & Spitzer, L. 1997, ApJ, 475, 623
- Fukugita, M., Hogan, C. J., & Peebles, P. J. E. 1998, ApJ, 503, 518
- Ganguly, R., Bond, N. A., Charlton, J. C., Eracleous, M., Brandt, W. N., & Churchill, C. W. 2001, ApJ, 549, 133
- Gibson, B. K., Giroux, M. L., Penton, S. V., Putman, M. E., Stocke, J. T., & Shull, J. M. 2000, AJ, 120, 1830
- Grevesse, N., & Anders, E. 1989, in AIP Conf. Proc. 183, Cosmic Abundances of Matter, ed. C. J. Waddington (New York: AIP), 1

- Grevesse, N., & Noels, A. 1993, in *Origin and Evolution of the Elements*, ed. N. Prantzos, E. Vangioni-Flam, & M. Cassé (Cambridge: Cambridge University Press), 15
- Haardt, F., & Madau, P. 1996, *ApJ*, 461, 20
- Hamann, F., & Ferland, G. 1999, *ARA&A*, 37, 487
- Heckman, T. M., Lehnert, M. D., Strickland, D. K., & Armus, L. 2000, *ApJS*, 129, 493
- Heckman, T. M., Sembach, K. R., Meurer, G. R., Strickland, D. K., Martin, C. L., Calzetti, D., & Leitherer, C. 2001, *ApJ*, 554, 1021
- Hellsten, U., Gnedin, N. Y., & Miralda-Escudé 1998, *ApJ*, 509, 56
- Holweger, H. 2001, in *Solar and Galactic Composition*, ed. R. F. Wimmer-Schweingruber (Berlin: Springer), in press
- Hwang, U., Mushotzky, R. F., Burns, J. O., Fukazawa, Y., & White, R. A. 1999, *ApJ*, 516, 604
- Jenkins, E. B. 1978, *ApJ*, 219, 845
- Kerr, F. J., & Lynden-Bell, D. 1986, *MNRAS*, 221, 1023
- Kimble, R. A., et al. 1998, *ApJ*, 492, L83
- Kulkarni, V. P., & Fall, S. M. 1993, *ApJ*, 413, L63
- Kuntz, K. D., Snowden, S. L., & Mushotzky, R. F. 2001, *ApJ*, 548, L119
- Mac Low, M.-M., & Ferrara, A. 1999, *ApJ*, 513, 142
- Maloney, P. 1993, *ApJ*, 414, 41
- McKee, C. F., & Hollenbach, D. J. 1980, *ARA&A*, 18, 219
- Moos, H. W., et al. 2000, *ApJ*, 538, L1
- Morton, D. C. 1991, *ApJS*, 77, 119
- Morton, D. C. 2001, in preparation
- Mulchaey, J. S. 2000, *ARA&A*, 38, 289
- Mulchaey, J. S., Davis, D. S., Mushotzky, R. F., & Burstein, D. 1996a, *ApJ*, 456, 80
- Mulchaey, J. S., Mushotzky, R. F., Burstein, D., Davis, D. S. 1996b, *ApJ*, 456, L5
- Oegerle, W. R., Tripp, T. M., Sembach, K. R., Jenkins, E. B., Bowen, D. V., Cowie, L. L., Green, R. F., Kruk, J. W., Savage, B. D., Shull, J. M., & York, D. G. 2000, *ApJ*, 538, L23
- Papovich, C., Norman, C., Bowen, D. V., Heckman, T., Savaglio, S., Koekemoer, A. M., & Blades, J. C. 2000, *ApJ*, 531, 654
- Penton, S. V., Shull, J. M., & Stocke, J. T. 2000, *ApJ*, 544, 150
- Perna, P., & Loeb, A. 1998, *ApJ*, 503, L135
- Pettini, M., Shapley, A. E., Steidel, C. C., Cuby, J.-G., Dickinson, M., Moorwood, A. F. M., Adelberger, K. L., & Giavalisco, M. 2001, *ApJ*, 554, 981
- Phillips, L. A., Ostriker, J. P., & Cen, R. 2001, *ApJ*, 554, L9
- Persic, M., & Salucci, P. 1992, *MNRAS*, 258, 14P
- Rauch, M., Miralda-Escudé, J., Sargent, W.L.W., Barlow, T.A., Hernquist, L., Weinberg D.H., Katz, N., Cen, R., Ostriker, J.P. 1997b, *ApJ*, 489, 7
- Richter, P., Sembach, K. R., Wakker, B. P., Savage, B. D., Tripp, T. M., Murphy, E. B., Kalberla, P. M. W., & Jenkins, E. B. 2001, *ApJ*, in press (astro-ph/0105466)
- Rines, K., Mahdavi, A., Geller, M. J., Diaferio, A., Mohr, J. J., & Wegner, G. 2001, *ApJ*, 555, 558
- Robertson, J. G. 1986, *PASP*, 98, 2000
- Sahnow, D. J., et al. 2000, *ApJ*, 538, L7
- Savage, B. D., et al. 2000, *ApJ*, 538, L27
- Savage, B. D., Sembach, K. R., Tripp, T. M., & Richter, P. 2001, *ApJ*, submitted
- Savage, B. D., & Sembach, K. R. 1991, *ApJ*, 379, 245
- Savage, B. D., Tripp, T. M., & Lu, L. 1998, *AJ*, 115, 436

- Scharf, C., Donahue, M., Voit, G. M., Rosati, P., & Postman, M. 2000, 528, L73
- Schaye, J. 2001, *ApJ*, in press (astro-ph/0104272)
- Sembach, K. R., et al. 2000, *ApJ*, 538, L31
- Sembach, K. R., & Savage, B. D. 1992, *ApJS*, 83, 147
- Shapiro, P. R., & Bahcall, J. N. 1980, *ApJ*, 241, 1
- Shull, J. M., Penton, S. V., Stocke, J. T., Giroux, M. L., van Gorkom, J. H., Lee, Y. H., & Carilli, C. 1999a, *AJ*, 116, 2094
- Shull, J. M., Roberts, D., Giroux, M. L., Penton, S. V., & Fardal, M. A. 1999b, *AJ*, 118, 1450
- Shull, J. M., Stocke, J. T., & Penton, S. V. 1996, *AJ*, 111, 72
- Sofia, U. J., & Meyer, D. M. 2001, *ApJ*, 554, L221
- Strickland, D. K., & Stevens, I. R. 2000, *MNRAS*, 314, 511
- Sutherland, R. S., & Dopita, M. A. 1993, *ApJS*, 88, 253
- Tripp, T. M. 2002, in ASP Conf. Ser. Extragalactic Gas at Low Redshift, A Workshop in Honor of Ray Weymann, ed. J. S. Mulchaey & J. Stocke (San Francisco: ASP), in press (astro-ph/0108278)
- Tripp, T. M., Lu, L., & Savage, B. D. 1998, *ApJ*, 508, 200
- Tripp, T. M., & Savage, B. D. 2000, *ApJ*, 542, 42
- Tripp, T. M., Savage, B. D., & Jenkins, E. B. 2000, 534, L1
- Tumlinson, J., Giroux, M. L., Shull, J. M., & Stocke, J. T. 1999, *AJ*, 118, 2148
- Verner, D. A., Tytler, D., & Barthel, P. D. 1994, *ApJ*, 430, 186
- Vogel, S., Weymann, R., Rauch, M., & Hamilton, T. 1995, *ApJ*, 441, 162
- Voit, G. M., Evrard, A. E., & Bryan, G. L. 2001, *ApJ*, 548, L123
- Wakker, B. P., et al. 1999, *Nature*, 402, 388
- Weinberg, D. H., Hernquist, L., Miralda-Escudé, J., & Katz, N., 1997, *ApJ*, 490, 564
- Woodgate, B. E., et al. 1998, *PASP*, 110, 1183
- Zabludoff, A. I., & Mulchaey, J. S. 1998, *ApJ*, 496, 39

